Retrieval of the scattering and microphysical properties of aerosols from ground-based optical measurements including polarization. I. Method

Anne Vermeulen, Claude Devaux, and Maurice Herman

A method has been developed for retrieving the scattering and microphysical properties of atmospheric aerosol from measurements of solar transmission, aureole, and angular distribution of the scattered and polarized sky light in the solar principal plane. Numerical simulations of measurements have been used to investigate the feasibility of the method and to test the algorithm's performance. It is shown that the absorption and scattering properties of an aerosol, i.e., the single-scattering albedo, the phase function, and the polarization for single scattering of incident unpolarized light, can be obtained by use of radiative transfer calculations to correct the values of scattered radiance and polarized radiance for multiple scattering, Rayleigh scattering, and the influence of ground. The method requires only measurement of the aerosol's optical thickness and an estimate of the ground's reflectance and does not need any specific assumption about properties of the aerosol. The accuracy of the retrieved phase function and polarization of the aerosols is examined at near-infrared wavelengths (e.g., 0.870 μm). The aerosol's microphysical properties (size distribution and complex refractive index) are derived in a second step. The real part of the refractive index is a strong function of the polarization, whereas the imaginary part is strongly dependent on the sky's radiance and the retrieved single-scattering albedo. It is demonstrated that inclusion of polarization data yields the real part of the refractive index.

OCIS codes: 280.1310, 010.1110, 260.5430, 290.4210.

1. Introduction

The characterization of terrestrial aerosols on a global scale is essential for assessing the climatic effect of aerosols and for satellite remote-sensing applications. The new generation of sensors [e.g., Polarization and directionality of the Earth's reflectances[1] (POLDER), Moderate Resolution Imaging Spectrometer (MODIS), and Multiangle Imaging Spectroradiometer[2] (MISR)] with improved radiometric and geometric performance is expected to provide high-accuracy multispectral, multiple-viewing-angle and polarization data of the Earth's atmosphere and surfaces. Some insight into the physical and chemical properties of the aerosols in addition to the aerosols' spectral optical thickness can be extracted from space observations.[3,4] In this context, ground-based observations of the aerosols in the solar spectral range play a major role: they help in the development and validation of spaceborne experiments devoted either to aerosol monitoring or to the elimination of aerosol effects for remote sensing of the Earth's surface.[5–7] Whereas satellite observations are made mostly in the backscattering direction and are contaminated by an important surface contribution, ground observations can include direct solar measurement, forward scattering, and backscattering and are less influenced by surface reflection. Direct monitoring of the aerosols from ground-based measurements acquired as part of intensive field measurement campaigns or as planned in the development of radiometer networks,[8] provides access to more key parameters than can be retrieved from satellite imagery.

Over the past decades, considerable effort has been devoted to the development of more-reliable ground-based instruments and to improvement of inversion

When this research was performed, all the authors were with the Laboratoire d'Optique Atmosphérique, Unité Mixte de Recherche 8518, Université des Sciences et Techniques de Lille, Unité de Formation et Recherche de Physique, 59655 Villeneuve d'Ascq, France. A. Vermeulen (anne@aeronet.gsfc.nasa.gov) is now with the Laboratory for Terrestrial Physics, NASA Goddard Space Flight Center, Code 923, 20771 Greenbelt, Maryland 20771.

Received 4 August 2000; revised manuscript received 4 August 2000.

0003-6935/00/336207-14$15.00/0

methods for retrieving the properties of aerosols. Measurements of the spectral aerosol's optical thickness, derived from solar transmission, are common and can be achieved with good accuracy with well-calibrated instruments. Measurement of solar aureole radiance is also common and useful. It permits derivation of the forward part of the aerosol's phase function. The aerosol's size distribution may be retrieved from these measurements.[9–14] Several authors, who generally use measurements in the solar almucantar, have emphasized the usefulness of extending sky radiance measurements to larger scattering angles. Kaufman *et al.*[15] used almucantar measurements up to the scattering angle of 120° to retrieve phase function and size distribution, following the procedure of Nakajima *et al.*[16] Moreover, Wang and Gordon[17] and Devaux *et al.*[18] showed that measurements of the sky radiance in a sufficiently large range of scattering angles allow one to derive the aerosol's single-scattering albedo, whereas analysis of multiwavelength measurements of the phase function and the spectral extinction may provide an indication of the particle's refractive index.[19–21]

In this paper we consider extended ground-based observations of the aerosols that involve, in addition to transmission and aureole measurements, the angular distribution of sky radiance and its polarization in the solar principal plane. These measurements have received less attention than have transmission and aureole measurements. Measurements of sky radiance in the solar principal plane allow one to retrieve the aerosol phase function for an extended range of scattering angles that provides information about aerosols with smaller dimensions.[22] Likewise, polarized sky radiance is known to be highly sensitive to the presence of aerosols in the Earth's atmosphere, as was shown by Sekera,[23] and may provide information on the refractive index of aerosols as shown both by calculations[22–25] and by balloonborne and ground-based measurements.[26–29] The data processing of measurements in the solar principal plane is more complicated than for transmission and aureole measurements, however, because of the increasing influence of multiple scattering and ground reflectance at large scattering angles. Moreover, because molecules are highly efficient in generating polarized light, they can largely mask the aerosol's polarized signature. The retrieval of the aerosol's scattering properties at large scattering angles, therefore, requires an accurate correction to eliminate the effects of ground reflectance and molecular and multiple scattering on the measurements.

In the present paper we propose a retrieval scheme for deriving the scattering and microphysical properties of aerosols by use of solar transmission measurements combined with the angular distribution of the sky radiance and its polarization in the aureole and the solar principal plane.

In a first step, the aerosol scattering properties, i.e., the single-scattering albedo, phase function, and polarization for single scattering of incident unpolarized light, are derived simultaneously. This procedure is addressed in Section 2. This step requires a correction for molecular scattering, multiple scattering, and ground influence in the radiance and polarization measurements. One uses appropriate radiative transfer calculations to evaluate and remove these contributions from the measurements. The correction of the radiance measurements was addressed previously by Devaux *et al.*[18] for the retrieval of the aerosol single-scattering albedo. Here we extend the method to the correction of the polarization measurements, and the sensitivity of the retrieval scheme is examined by use of synthetic ground-based data sets.

In a second step, the aerosol's size distribution and refractive index are derived simultaneously from their scattering properties. This step is addressed in Section 3. Given the aerosol's refractive index, the retrieval of the aerosol size distribution is achieved with an inversion method adapted from the method of King *et al.*[9] to include the phase function and the polarization data (Subsection 3.A). Refractive-index retrieval is examined in Subsection 3.B. The real part of the refractive index depends principally on the polarization, whereas one obtains the imaginary part by comparing the calculated and the measured single-scattering albedos. It is shown that the polarization provides the real part of the refractive index. Comparison of retrievals made with and without polarization data show that in some cases the inclusion of polarization will provide for significantly better retrievals of the small radius size distribution.

We examine the validation of the scheme by using numerical simulations of the measurements. We consider measurements performed at a near-infrared wavelength, 0.870 μm, to minimize the influence of molecular scattering. Application of the scheme to experimental data will be addressed in a future paper.

2. Retrieval of the Aerosol Scattering Properties

A. Sensitivity of Total and Polarized Radiances to Multiple Scattering, Molecular Scattering, and Ground Reflectance

We intend to retrieve the aerosol scattering properties in an extended range of scattering angles, Θ, by performing measurements in the solar principal plane at low solar elevation. Typically, we consider that the total radiance and the polarized radiance are measured from scattering angles that range from 2° to 20–30° in the solar aureole and that there is a total and polarized radiance from 20° to $\Theta_{\max}$ in the principal-plane geometry. The smaller angles (2° and 20°) correspond to the lower limits of the aureolemeter and the radiopolarimeter, respectively; $\Theta_{\max}$ corresponds to the maximum value accessible in the principal-plane geometry, that is,

$$\Theta_{\max} = \theta_S + \theta_{V\max}, \tag{1}$$

where θ_S is the Sun's zenith angle and $\theta_{V\max}$ is the largest zenith view angle, usually ~80°. At low Sun

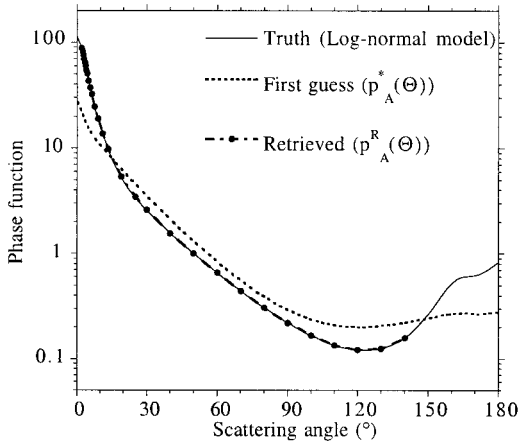

Fig. 1. True aerosol phase function, the phase function of the bimodal log-normal model, compared with the phase function of the Junge model, taken as the first guess $p^*_A(\Theta)$ in the retrieval scheme. The retrieved phase function $p^R_A(\Theta)$ is also shown.

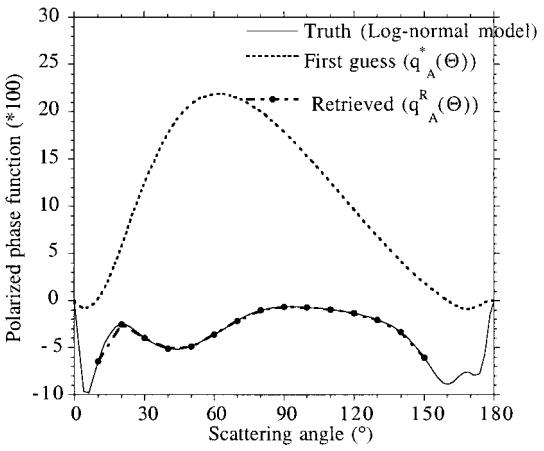

Fig. 2. Same as Fig. 1 but for the polarized phase function.

elevation, backscattering directions can be reached (e.g., $\Theta_{\max} \sim 145°$ for $\theta_S = 65°$).

Although the contributions of ground reflectance, multiple scattering, and molecular scattering are negligible or small in measurements of solar transmission and aureole, they have increasing importance for observations at large scattering angles. Let us illustrate this from numerical simulations of the sky's radiance field for a typical example.

The calculations correspond to those for aerosols with optical thickness for extinction $\tau_A = 0.1$ and single-scattering albedo $\omega_0 = 0.85$ at the wavelength considered, $\lambda = 0.870$ μm, so the molecular optical thickness is $\tau_M = 0.015$. The aerosol's phase matrix is derived from Mie theory for spherical particles with real refractive index $m_r = 1.40$ and the size distribution given by the Junge model [$n(r) \sim r^{-\upsilon}$, where r is the particle radius] with parameter $\upsilon = 4.6$.

To account for the polarization properties of the particles, we made calculations of the Stokes parameters of the radiation field, using the aerosol phase matrix[30] in the form

$$\begin{bmatrix} P_{11}(\Theta) & P_{12}(\Theta) & 0 & 0 \\ P_{12}(\Theta) & P_{22}(\Theta) & 0 & 0 \\ 0 & 0 & P_{33}(\Theta) & P_{34}(\Theta) \\ 0 & 0 & P_{34}(\Theta) & P_{44}(\Theta) \end{bmatrix}. \quad (2)$$

Of course, although the measurements depend on all the terms of the aerosol phase matrix by way of the multiple-scattering processes, we intend to retrieve only the terms that intervene in the single-scattering process from the incident unpolarized solar beam, that is, $P_{11}(\Theta)$ and $P_{12}(\Theta)$. Moreover, because the ellipticity is known to be negligible,[31] we make the calculations here by neglecting the fourth row and the fourth column of the phase matrix.

For the Junge model of particles, the phase function $p_A(\Theta)$ at $\lambda = 0.870$ μm [i.e., the $P_{11}(\Theta)$ term in expression (2)] is illustrated in Fig. 1 (small dotted curve). Here, $q_A(\Theta)$ stands for $P_{21}(\Theta)$ [such that the degree of polarization for single scattering is $P_{21}(\Theta)/P_{11}(\Theta)$]. The function $q_A(\Theta)$ at $\lambda = 0.870$ μm, hereafter designated the aerosol's polarized phase function, is shown in Fig. 2 (small-dotted curve). As usual, $q_A(\Theta)$ is positive for linear polarization perpendicular to the scattering plane (as in the molecular case) and negative for polarization parallel to the scattering plane.[22]

The simulations are performed by a successive-order-of-scattering[32] (SOS) code. We assume a plane-parallel atmosphere on top of a Lambertian ground surface with uniform reflectance $\rho_g = 0.30$, a typical value of ground reflectance at the near-infrared wavelength considered. The aerosols are mixed uniformly with the molecules. The code accounts for multiple scattering by molecules and aerosols and reflection on the surface. Polarization ellipticity is neglected. The results are expressed in terms of normalized radiance L and normalized polarized radiance L_p, defined by

$$L = \pi L^*/E, \quad (3)$$

where L^* is the sky radiance that reaches the radiometer in the viewing direction θ_v and E is the extraterrestrial solar irradiance.

Figure 3(a) shows the calculated sky radiance L in the principal plane (i.e., for azimuth angles $\phi = 0°$ and $\phi = 180°$) as a function of the zenith viewing angle. For comparison, we have shown in this figure the sky radiance calculated for the same conditions but with the ground reflectance (i.e., $\rho_g = 0.0$ in the SOS code), the ground reflectance and the molecular scattering (i.e., $\rho_g = 0.0$ and $\tau_M = 0.0$ in the SOS code), and the ground reflectance and the aerosol scattering (i.e., with $\rho_g = 0.0$ and $\tau_A = 0.0$ in the SOS code) neglected. Figure 3(a) shows that the molecular scattering and the radiance reflected by the ground and rescattered into the radiometer's field of view can significantly affect the measurements.

The polarized sky radiance L_p is shown similarly in Fig. 3(b). Inasmuch as we consider measurements in the solar principal plane, consideration of symmetry shows that the polarized vibration is linear, either

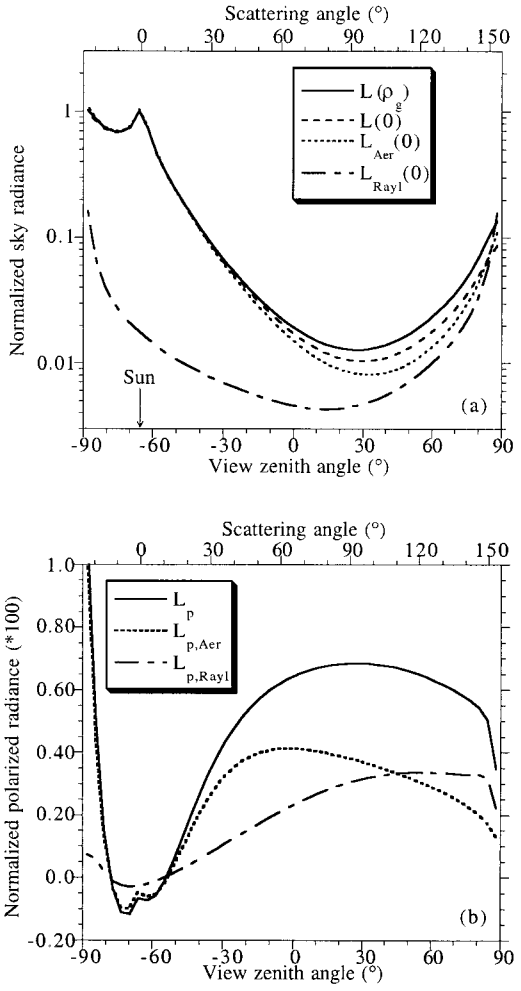

Fig. 3. (a) Effect of aerosol scattering, molecular scattering, and ground reflectance on the sky radiance. Radiance $L(\rho_g)$ is calculated for typical experimental conditions ($\tau_A = 0.1$ and $\omega_0 = 0.85$ at $\lambda = 0.870$ μm; $\theta_s = 65°$). The radiance is compared with calculations with $\rho_g = 0$ [$L(0)$], with calculations with $\rho_g = 0$ and $\tau_M = 0$ [$L_{\mathrm{Aer}}(0)$], and with $\rho_g = 0$ and $\tau_A = 0$ [$L_{\mathrm{Rayl}}(0)$]. The result corresponds to observations in the solar principal plane, and is shown as a function of the view's zenith angle. This figure shows that the molecular scattering and the radiance reflected by the ground and rescattered into the radiometer's field of view can contribute significantly to the radiance and polarized radiance measurements. (b) Same conditions as in (a): atmospheric (i.e., molecules and aerosols) polarized radiance (L_p), polarized radiance that is due solely to molecules ($L_{p,\mathrm{Rayl}}$), and polarized radiance that is due solely to aerosols ($L_{p,\mathrm{Aer}}$). The large influence of molecular scattering on polarized light is shown.

perpendicular or parallel to the solar principal plane. We then consider that the corresponding polarized radiance L_p is, respectively, positive or negative. For comparison we also show in Fig. 3(b) the polarized sky radiance calculated for the same conditions but with the molecular polarization neglected (in the SOS code, we let the aerosols and the molecules scatter but we let only the aerosols polarize) and with the aerosol polarization neglected (in the SOS code we let the aerosols and the molecules scatter but we let only the molecules polarize). It is interesting to note

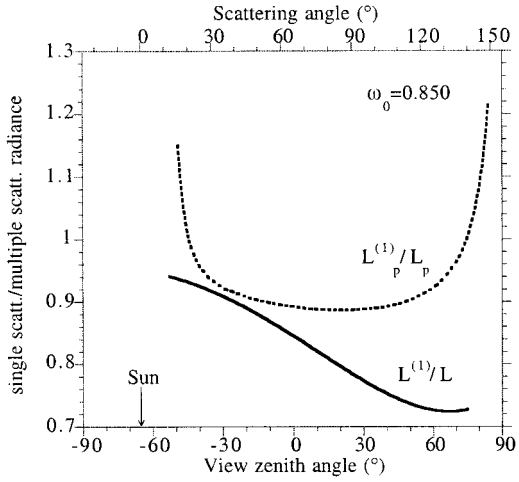

Fig. 4. Relative contribution of single scattering to total radiance $[L^{(1)}/L]$ and to polarized radiance $[L_p^{(1)}/L_p]$, showing that the influence of multiple scattering is significant in the radiance and to a lesser extent in the polarized radiance, especially toward large scattering angles.

that, unlike with radiance, the aerosol and molecular polarized radiance is not coupled (the polarized sky radiance that is solely due to aerosols and the one that is due solely to molecules sum to the total atmospheric polarized radiance L_p). Also note that, as discussed in Subsection 2.B below, the polarized sky radiance does not depend on the ground-reflecting properties. Figure 3(b) illustrates the large influence of molecular scattering on polarized light. In spite of use of a near-infrared wavelength to minimize Rayleigh effects, the polarization that is due to molecular scattering can largely dominate and mask the aerosol signature.

Finally, Fig. 4 illustrates the influence of multiple scattering. Let us define the radiance and the polarized radiance that corresponds to single scattering from the unpolarized solar beam [$L^{(1)}$ and $L_p^{(1)}$ respectively] by

$$L^{(1)}(\Theta) = \frac{1}{4 \cos \theta_v}[\tau_M p_M(\Theta) + \omega_0 \tau_A p_A(\Theta)], \qquad (4)$$

$$L_p^{(1)}(\Theta) = \frac{1}{4 \cos \theta_v}[\tau_M q_M(\Theta) + \omega_0 \tau_A q_A(\Theta)], \qquad (5)$$

where p_M and q_M are the molecular phase function and the molecular polarized phase function, respectively.

Figure 4 shows the ratios $L^{(1)}/L$ and $L_p^{(1)}/L_p$ versus the view angle θ_v for observations in the principal plane. The influence of multiple scattering is significant in the radiance, and to a lesser extent in the polarized radiance, especially toward large scattering angles. For aerosols with smaller dimensions, larger optical depth, or both, the amount of multiple polarized radiance can contribute to approximately 30–40% of the total polarized light.[33]

B. Description of the Method

Let us examine how the aerosol scattering properties, that is, the albedo for single scattering, ω_0, phase function $p_A(\Theta)$, and polarized phase function $q_A(\Theta)$, are retrieved from the measurements. The method has been detailed by Devaux *et al.*[18] for radiance measurements.

Schematically, the method consists in eliminating successively the ground contribution and the multiple-scattering contribution to the measurements to retrieve the single-scattering contributions of the atmosphere in the form of Eqs. (4) and (5). Then, because the molecular terms are known in these equations, the aerosol terms $\omega_0 p_A(\Theta)$ and $\omega_0 q_A(\Theta)$ are derived. Provided that measurements are obtained over a sufficient range of scattering angle because of the normalization of $p_A(\Theta)$, the single-scattering albedo is derived from

$$\omega_0 = \int [\omega_0 p_A(\Theta)] \sin \Theta d\Theta/2, \tag{6}$$

which leads to derivation of the aerosol phase function and the polarized phase function.

The contributions to the method made by ground reflectance and multiple scattering in the sky radiance are estimated from radiative transfer calculations with the SOS code. Clearly, these contributions depend directly on the aerosol's optical thickness and on the ground reflectance. However, it may be expected that these calculations may be much less sensitive to the exact properties of the aerosol scattering matrix. We assume here that the aerosol's optical thickness has been derived from the transmission measurement and that an estimate of the ground reflectance over the area where the measurements are performed is known. Let τ_A^* and ρ_g^* stand for these respective estimates. Then some initial guess has to be made for the aerosol phase matrix P_A^*. The choice for the guess for the phase matrix is considered in Subsection 2.C below, in parallel with the effects of the uncertainties in the inputs of τ_A^* and ρ_g^* in the SOS code. Finally, because the calculated influences depend on the unknown value of ω_0, let ω_0^* be the guess for the aerosol single-scattering albedo.

The first step in the correction of the sky radiance measurements consists of subtracting the ground influence. Let L^* and L_0^* stand for computations of the sky radiance performed with the estimate of the ground reflectance ρ_g^* and with $\rho_g^* = 0$ as the lower boundary condition [i.e., $L^* = L^*(\tau_A^*, \omega_0^*, P_A^*, \rho_g^*)$ and $L_0^* = L^*(\tau_A^*, \omega_0^*, P_A^*, 0)$]. Clearly, L^* differs from L_0^* only in the number of photons that have been reflected by the ground, and the correction for the ground contribution in the measurements is approximately

$$\Delta L^* = L^* - L_0^*. \tag{7}$$

In the second step, the atmospheric term, i.e., $L - \Delta L^*$, is corrected for multiple scattering in the atmosphere. Provided that the molecular and the aerosol parameters are nearly the same in the calculations and in the measurements, we expect that the (single scattering)/(total scattering) ratio will be nearly the same for calculations and measurements; that is,

$$\frac{(\omega_0 \tau_A p_A + \tau_M p_M)/4 \cos \theta_v}{L - \Delta L^*} = \frac{(\omega_0^* \tau_A^* p_A^* + \tau_M p_M)/4 \cos \theta_v}{L_0^*}, \tag{8}$$

or, with a simple transformation,

$$\omega_0 \tau_A p_A = \frac{L - \Delta L^*}{L_0^*} \omega_0^* \tau_A^* p_A^* + \frac{L - L^*}{L_0^*} \tau_M p_M. \tag{9}$$

Finally, by neglecting the difference between the true and the measured aerosol optical thickness, we find from Eq. (9) that

$$\frac{\omega_0}{\omega_0^*} p_A = \frac{L - \Delta L^*}{L_0^*} p_A^* + \frac{L - L^*}{L_0^*} \frac{\tau_M}{\omega_0^* \tau_A^*} p_M. \tag{10}$$

Note that, because transmission measurements can be highly accurate, the measured aerosol optical thickness τ_A^* should be near the exact value τ_A. Finally, Eq. (10) is the basic equation that we used for our retrieval. Its validity is assessed in Subsection 2.C below.

Now Eq. (10) is used first to retrieve the aerosol single-scattering albedo. The right-hand side of Eq. (10) is calculated for several values of ω_0^* and the resulting integral, i.e.,

$$Y(\omega_0^*) = \int_0^\pi \left(\frac{L - \Delta L^*}{L_0^*} p_A^* + \frac{L - L^*}{L_0^*} \frac{\tau_M}{\omega_0^* \tau_A^*} p_M \right) \sin \Theta d\Theta, \tag{11}$$

is estimated. Because $Y(\omega_0^*) = 2\omega_0/\omega_0^*$, according to the normalization of p_A the retrieved single-scattering albedo ω_0^R is this value of ω_0^* for which $Y(\omega_0^R) = 2$.

In practice, Eq. (10) defines $Y(\omega_0^*)$ only within the range of scattering angles where the $L(\Theta)$ measurements are performed. The missing data in the forward-scattering [0°–2°] and the backscattering (Θ_{max}, 180°) ranges usually contribute less than a few percent to the calculation of the integral, and we use the initial guess $p_A^*(\Theta)$ to extrapolate $Y(\omega_0^*)$ in these missing directions.

Then we retrieve the aerosol phase function, $p_A^R(\Theta)$, by substituting the retrieved albedo into Eq. (10), i.e.,

$$p_A^R = \frac{L - \Delta L^*(\omega_0^R)}{L_0^*(\omega_0^R)} p_A^* + \frac{L - L^*(\omega_0^R)}{L_0^*(\omega_0^R)} \frac{\tau_M}{\omega_0^R \tau_A^*} p_M. \tag{12}$$

Finally, we apply a similar scheme to the measurements of polarized radiance to retrieve the aerosol polarized phase function. The process is simpler. Because scattering of the nearly isotropic light reflected from the ground has negligible polarization,[34] no correction for ground contamination to the polarized radiance is needed. The influence of the ground

reflectance and polarization on the polarized sky radiance was investigated by Lafrance.[35] Numerical simulations performed with realistic reflectances and bidirectional polarization distribution functions of the ground show that the error in L_p is no more than approximately 1–2% when the ground influence is neglected. The polarized measurements, therefore, are directly corrected for multiple-scattering effects according to the previous scheme, except that the calculations are performed only for the retrieved aerosol single-scattering albedo. Let L_p^* be the polarized sky radiance calculated with the initial-guess aerosol model and the retrieved albedo for single scattering, ω_0^R. With $q_A^*(\Theta)$ and $q_M(\Theta)$ in place of $p_A^*(\Theta)$ and $p_M(\Theta)$ for polarized light, the retrieved polarized phase function of the aerosols is therefore

$$q_A^R = \frac{L_p}{L_p^*(\omega_0^R)}\, q_A^* + \frac{L_p - L_p^*(\omega_0^R)}{L_p^*(\omega_0^R)}\, \frac{\tau_M}{\omega_0^R \tau_A^*}\, q_M. \qquad (13)$$

The whole retrieval scheme, involving measurements and computations, is summarized in Fig. 5.

C. Validation of the Method

To validate the method, we perform numerical simulations of sky radiances L and L_p for a known aerosol model. First, we suppose that the aerosol optical thickness for extinction and the ground reflectance are known and neglect the measurement errors in the sky radiance. We choose some simple guess for aerosol phase matrix $P_A^*(\Theta)$. Then the simulated measurements are entered into Eqs. (10)–(13) and the $p_A^R(\Theta)$ and $q_A^R(\Theta)$ retrievals are compared with the inputs. We do not discuss the intermediate retrieval of ω_0^R, which has been examined in Devaux *et al.*[18] Second, we examine the influence on $p_A^R(\Theta)$ and $q_A^R(\Theta)$ of measurement errors in τ_A^*, ρ_g^*, L, and L_p. Note that, because the aerosol's vertical density profile is unknown, we calculate the sky radiances L^*, L_0^*, and L_p^* in Eqs. (10)–(13) by mixing aerosols and molecules according to scale heights 2 and 8 km, respectively.

1. *Guessed Aerosol Phase Matrix*

The choice for the first guess $P_A^*(\Theta)$ for the aerosol phase matrix is not important, as was shown by the simulations. Even when the estimated $P_A^*(\Theta)$ departs significantly from the true phase matrix (given by Mie theory applied to the model), $p_A^R(\Theta)$ and $q_A^R(\Theta)$ rapidly converge toward the true functions. In the second step of the inversion scheme, by processing ω_0^R, $p_A^R(\Theta)$, and $q_A^R(\Theta)$ as explained in Section 3, we fit these retrievals by a spherical aerosol model defined by m_r^R, m_i^R, and $n(r)$. Let $P_A^R(\Theta)$ be the corresponding phase matrix (see Fig. 6). Then, when we iterate the procedure by using $P_A^R(\Theta)$ as a new guess, the departures of ω_0^R, $p_A^R(\Theta)$, and $q_A^R(\Theta)$ from the true functions prove to be negligible, as we illustrate in Figs. 1 and 2. Numerical simulations of L and L_p were performed for a bimodal log-normal aerosol model as the sum of two log-normal distribution functions

$$n(r) = \frac{N}{\sqrt{2\pi} r \sigma} \exp\left[-\frac{(\ln r - \ln \bar{r})^2}{2\sigma^2} \right], \qquad (14)$$

with parameters $\bar{r}_1 = 0.10$ μm, $\sigma_1 = 0.405$, and $N_1 = 1$, and $\bar{r}_2 = 0.50$ μm, $\sigma_1 = 0.693$, and $N_2 = 0.03$, respectively, and refractive index $m = 1.50 - 0.001i$. The corresponding functions $p_A(\Theta)$ and $q_A(\Theta)$ at $\lambda = 870$ nm are illustrated in Figs. 1 and 2 (solid curves). The resultant albedo is $\omega_0 = 0.98$. The other inputs were $\tau_A = 0.40$ and $\rho_g = 0.30$. We assumed that $\theta_s = 70°$, with measurements performed until $\Theta = 150°$.

As a simple guess, we chose a Junge aerosol model of spherical particles, $n(r) = Cr^{-\upsilon}$, with the refractive index fixed arbitrarily as $m_r = 1.40$. The parameter υ may be adjusted, for example, to fit the measured angstrom exponent or the aureole measurements. Here we chose $\upsilon = 3.5$, which provides a rough agreement with the behavior of the aureole data. The corresponding guesses, $p_A^*(\Theta)$ and $q_A^*(\Theta)$, largely depart from the true functions, as shown in Figs. 1 and 2.

The simulated measurements were processed according to Eqs. (10)–(13) with the $P_A^*(\Theta)$ matrix corresponding to the Junge model, $m_r = 1.40$, $\upsilon = 3.5$, and the $p_A^R(\Theta)$ and $q_A^R(\Theta)$ retrievals are shown in Figs. 1 and 2. They compare well with the true functions. Processing of $p_A^R(\Theta)$ and $q_A^R(\Theta)$ according to the method explained in Section 3 below leads to an aerosol model that is quite close to the bimodal input, and iteration of the method with the corresponding phase matrix leads to a second retrieval of $p_A^R(\Theta)$ and $q_A^R(\Theta)$ that are indiscernible from the true functions except in directions where the measurements are extrapolated (i.e., [0–2°] and (Θ_{max}, 180°)], but note that these directions will not be used in the inversion processing described in Subsection 3.B.

2. *Effect of Measurement Errors*

The influence of the various measurement errors on phase function and polarized phase function retrievals is detailed in Figs. 7 and 8. The results correspond to the standard case of the Junge aerosol size distribution with parameter $\upsilon = 4.6$, with refractive index $m_r = 1.40$, used in Subsection 2.A. Measurements were simulated for $\tau_A = 0.1$, $\omega_0 = 0.85$, and $\theta_s = 65°$.

We shall not discuss further the error budget of the single-scattering albedo, which was examined by Devaux *et al.*[18] Let us just recall that the main source of error is an error in calibration of the sky radiance. Accordingly, the relative accuracy in the retrieved ω_0 is nearly equal to the relative accuracy in the radiance calibration. This calibration error, by contrast, does not significantly affect the phase function or the polarized phase function. We processed the simulated measurements again, using for $P_A^*(\Theta)$ the exact input corresponding to the Junge distribution but assuming a +10% or −10% systematic error in the

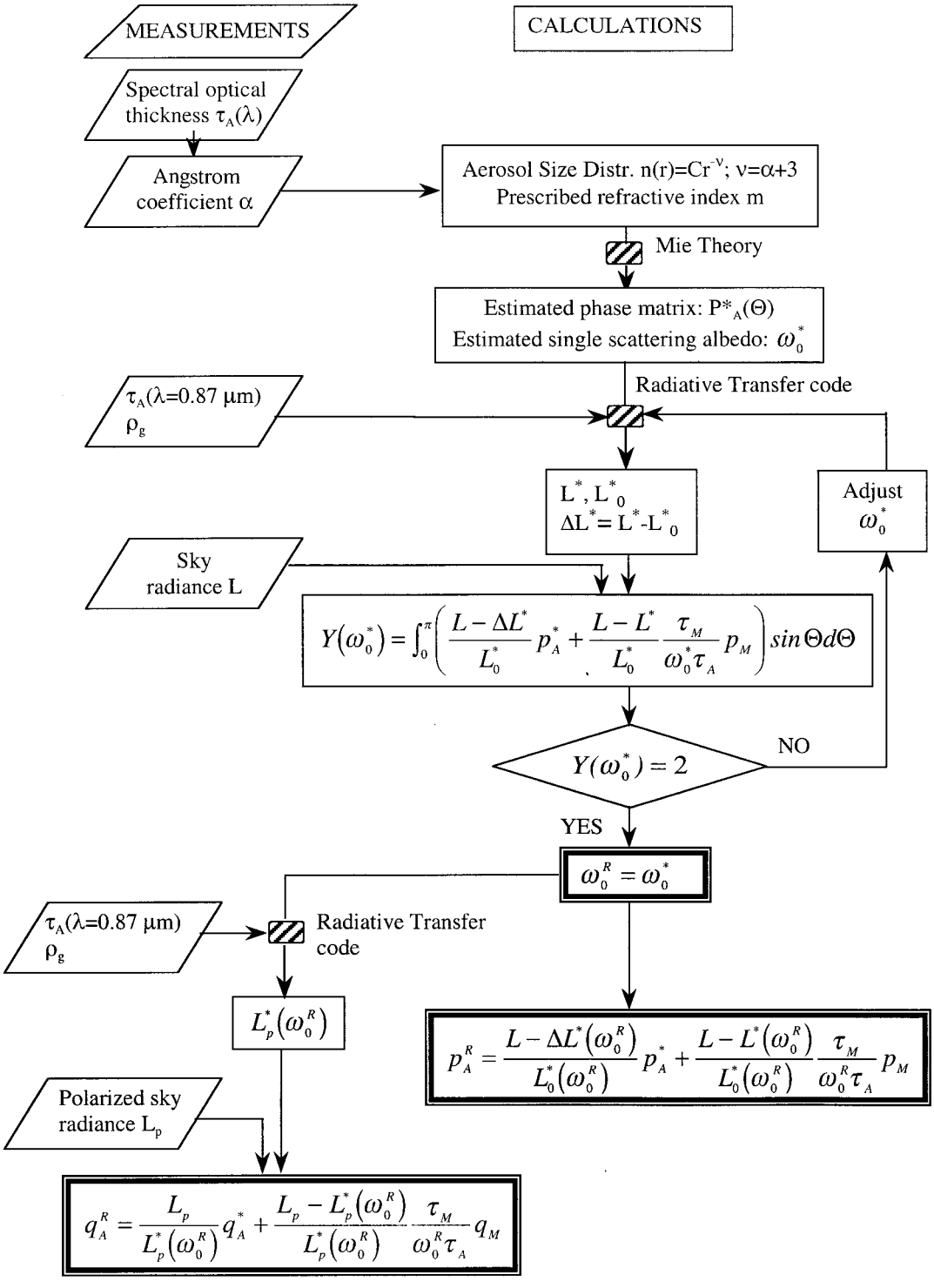

Fig. 5. Schematic description of the method for retrieving the aerosol scattering properties. The method uses measurements and calculations to retrieve the aerosol phase function, the polarized phase function, and the single-scattering albedo. A more-detailed description is given in Subsection 2.B.

radiance. This error directly affects the retrieved albedo; given the aerosol optical thickness for extinction, the change in the sky radiance estimate that is due to the calibration error entails an increase or a decrease in the estimated optical thickness for scattering of the aerosols. But the error entailed in the retrieved phase function is less than 2%, as shown in Fig. 7, and the error in the polarized phase function ranges from 2% to 10% for scattering angles below 120° and increases to 16% at 140°, as shown in Fig. 8.

The error in τ_A is the second source of uncertainty.

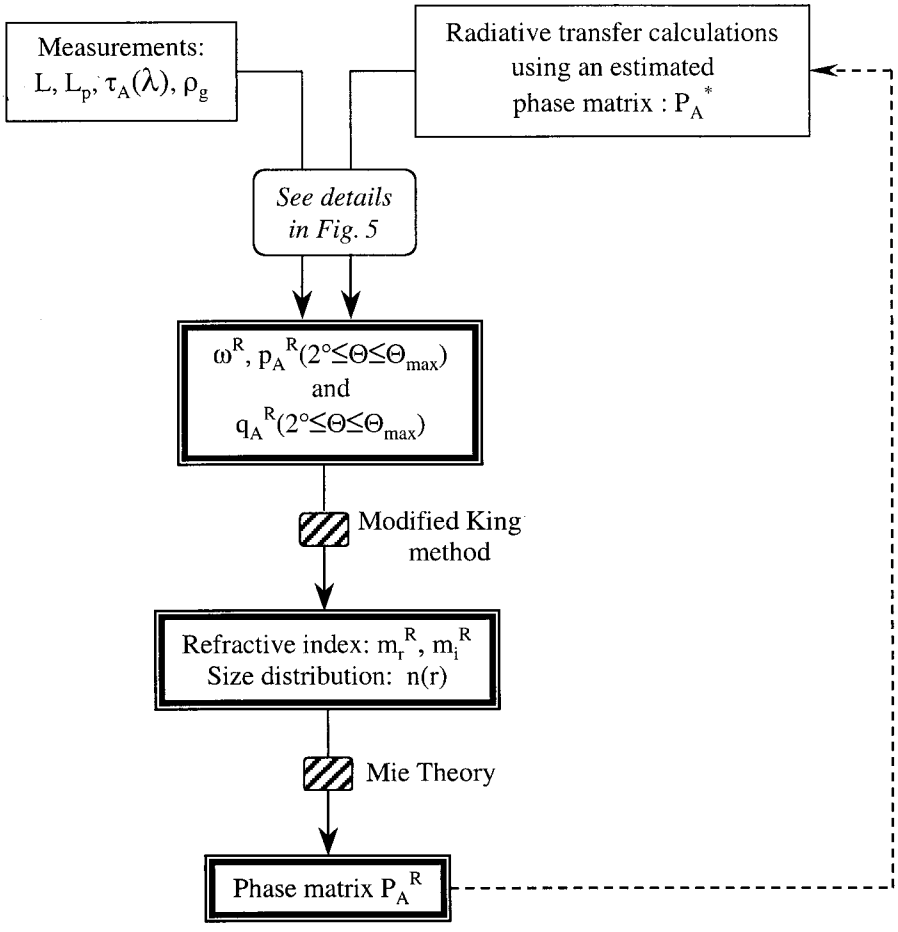

Fig. 6. Flow chart of the retrieval of aerosol properties.

We processed the inversion by now assuming a 10% error in τ_A. Although this assumption leads to approximately 7% error in ω_0, it does not significantly affect the phase function retrieval. The error is ~2% up to a 130° scattering angle and increases to 7% at 140° (Fig. 7). For the polarized phase function (Fig. 8), the error is ~1% below 120° and as much as 3.5% at 140°.

Finally, we performed the data processing by assuming a 10% error in the estimate of the ground reflectance. The influence on ω_0^R, $p_A^R(\Theta)$, and $q_A^R(\Theta)$ retrievals is less than 1% and is not shown in Figs. 7 and 8.

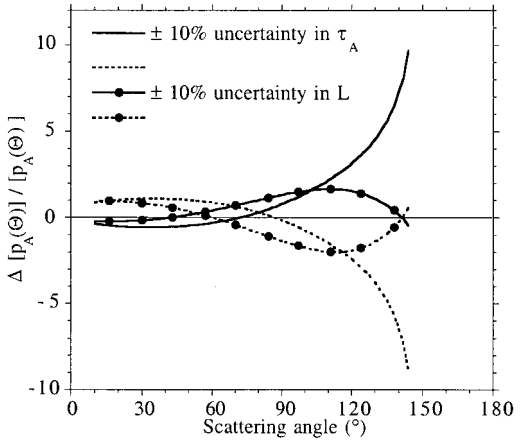

Fig. 7. Relative difference between the retrieved phase function and the true phase function for ±10% error in the radiance and in the aerosol optical thickness.

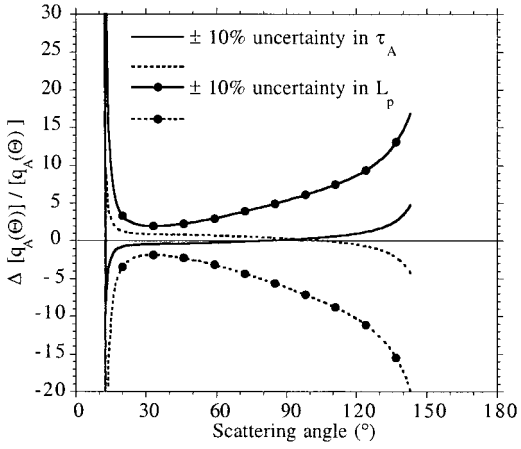

Fig. 8. Relative difference between the retrieved polarized phase function and the true polarized phase function for ±10% error in the polarized radiance and in the aerosol optical thickness.

3. Retrieval of Particle-Size Distribution and Refractive Index

We now consider the retrieval of the aerosol properties from their scattering features. We consider spherical particles. In Subsection 3.A we show how we derive their size distribution from phase function $p_A(\Theta)$ by assuming that the refractive index of the particles is known. The advantage of polarization measurements is discussed in Subsection 3.B, where we examine how both the particles' refractive index and size distribution may be retrieved from knowledge of ω_0, $p_A(\Theta)$, and $q_A(\Theta)$.

A. Retrieval of $n(r)$

The retrieval of the columnar aerosol size distribution from the measured phase function is made according to a modified form of the linear constrained method of King *et al.*[9] Their original method was modified to use the angular phase function instead of the spectral aerosol's optical thickness.

We assume spherical homogeneous particles and retrieve aerosol size distribution $n(r)$. We assume that $n(r)$ is normalized such that the resultant optical thickness is 1; i.e.,

$$\int_0^\infty \pi r^2 Q_{\mathrm{sca}}(r, \lambda, m) n(r) \mathrm{d}r = 1. \tag{15}$$

Thus the normalized aerosol phase function $p_A(\Theta_j)$ is given through Mie theory by

$$p_A(\Theta_j) = \int_{r_{\min}}^{r_{\max}} \pi r^2 Q_{\mathrm{sca}}(r, \lambda, m) p(\Theta_j, r, \lambda, m) n(r) \mathrm{d}r, \tag{16}$$

where $Q_{\mathrm{sca}}(r, \lambda, m)$ is the scattering efficiency factor, and $p(\Theta_j, r, \lambda, m)$ is the normalized phase function of a particle with radius r and refractive index m at the observation wavelength λ. We will assume that L and M measurement angles Θ_j are selected, respectively, in the aureole and principal plane ranges.

Following King *et al.*,[9] we replace the integral in Eq. (16) by a summation of partial integrals over N contiguous finite ranges of radii $[r_i - \Delta r_i/2,\ r_i + \Delta r_i/2]\ i = 1, N$, with $N < L + M$, and $n(r)$ is replaced by

$$n(r) = h(r) f(r), \tag{17}$$

where $h(r)$ and $f(r)$ are, respectively, a rapidly and a slowly varying function of r. Assuming that $f(r)$ is constant within each radius class, we obtain from Eq. (16)

$$\begin{aligned} p_A(\Theta_j) &= \sum_{i=1}^{N} f(r_i) \int_{r_1 - \Delta r_i/2}^{r_i + \Delta r_i/2} \pi r^2 Q_{\mathrm{sca}} p(\Theta_j) h(r) \mathrm{d}r \\ &= \sum_{i=1}^{N} A_{ji} f(r_i). \end{aligned} \tag{18}$$

Let $n^{(p)}(r_i)$ stand for the estimates of $n(r)$ at points r_i at iteration step p. We assume that, within each radius range $[r_i, r_{i+1}]$, $h(r)$ is in the form $h(r) = C_i^{(p)} r^{-v_i^{(p)}}$, with the $C_i^{(p)}$ and $v_i^{(p)}$ adjusted such that $h(r_i) = n^{(p)}(r_i)$. By using this form for $h(r)$, we calculate A_{ji} in Eq. (18) and derive the correction terms $f(r_i)$ from the system of linear equations

$$p_A = Af + \varepsilon, \tag{19}$$

which provides

$$n^{(p+1)}(r_i) = n^{(p)}(r_i) f(r_i). \tag{20}$$

The iteration starts with

$$n^{(0)}(r) = C r^{-v_0}, \tag{21}$$

where v_0 can be taken as $v_0 = \alpha + 3$, where α is the angstrom exponent and C is adjusted from Eq. (15). Moreover, whereas multispectral aerosol optical thicknesses have the same order of magnitude, the phase function can vary by 2 or 3 orders of magnitude from forward to backward scattering. Therefore we normalize the system of Eqs. (19) in the form

$$p_A^* = A^* f + \varepsilon, \tag{22}$$

where

$$p_A^*(\Theta_j) = p_A(\Theta_j)/\bar{A}_j, \qquad A_{ji}^* = A_{ji}/\bar{A}_j, \qquad \bar{A}_j = \sum_i A_{ji}. \tag{23}$$

The rms residual between the measured and the retrieved phase functions is calculated at the $K = L + M$ measurement points. The iterative procedure stops when the rms residual,

$$\sigma_p = \left\{ \frac{1}{K} \sum_{j=1}^{K} \left[\frac{p_A(\Theta_j) - p_A^{\mathrm{ret}}(\Theta_j)}{p_A(\Theta_j)} \right]^2 \right\}^{1/2}, \tag{24}$$

reaches a minimum or is of the same order of magnitude as the measurement and method errors. The convergence toward a solution requires that each element $p_A^*(\Theta_j)$, $j = 1, 2, \ldots, K$, as well as f_j, $j = 1, 2, \ldots, N$, converge to unity.

The selected scattering angles and classes of particle radius have to be optimized to prevent there being too many insignificant matrix elements A_{ji}^*. This optimization can be achieved from the typical behavior of $A^*(\Theta, r)$, as displayed in Fig. 9. In particular, the upper and lower limits $r_{\min}$ and $r_{\max}$ have to be adjusted, according to the observed particles, such that the contribution of at least one extreme matrix element will be a few percent of p_A^*; otherwise instabilities would develop. Typically, $n(r)$ is retrieved from $\sim r_{\min} = 0.03$ μm to $r_{\max} = 10.0$ μm, within 16 classes of radius, with 8 classes from $r_{\min}$ to 2 μm and 8 classes from 2 μm to $r_{\max}$.

B. Retrieval of $n(r)$ and m

1. Retrieval from Radiance Measurements Only

First we consider measurements of the solar extinction and sky radiance at one wavelength. As we

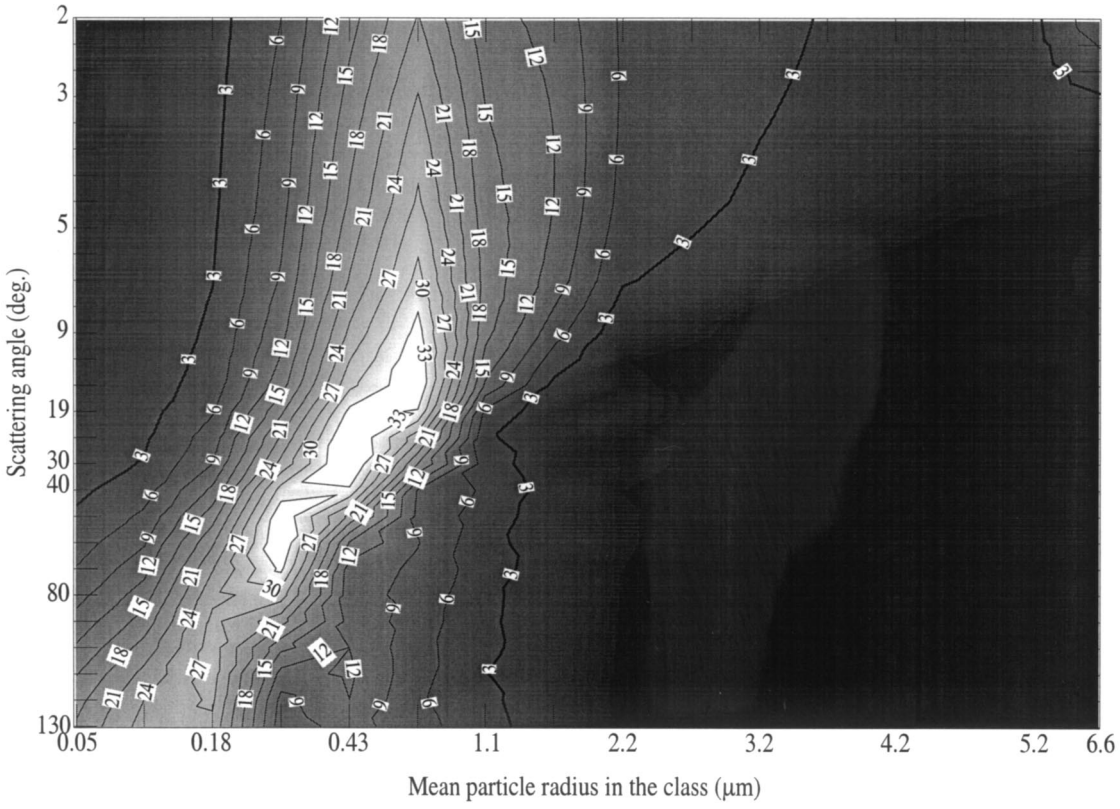

Fig. 9. Contribution (in percent) of each size interval to the phase function from 2° to 130°. Particles smaller than 0.1 μm (class 1) or with radii of 0.10 to 0.5 μm (classes 2–5) contribute the most to the phase function at large angles; large particles, above 0.8 μm (above class 8), contribute exclusively to the forward scattering.

explained above, we can derive the aerosol phase function $p_A(\Theta)$ and the albedo for single scattering ω_0 from these measurements. Then, by using the method described in Subsection 3.A, we can derive the size distribution of the aerosols, $n(r)$, from the phase function between 2° and $\Theta_{\max}$ (~140°). As the aerosol's refractive index is unknown, we examine how $n(r)$ varies according to the assumed refractive index. We consider only variation of the real part, m_r, of the refractive index; the imaginary part is adjusted to be consistent with the measured single-scattering albedo.

Let us consider again the standard Junge aerosol model of Subsection 2.A: $v = 4.6$, with refractive index $m_r = 1.40$. Assuming exact retrieval of the aerosol phase function within the range [2°, 130°], let us apply the previous scheme to $p_A(\Theta)$ by varying m_r from 1.30 to 1.50 in steps of 0.05, including the true index 1.40. Whatever index is used, a stable solution is reached after only a few iterations (usually four), and thus one can achieve a good fit to the phase function. Figure 10 shows the retrieved volume size distributions $dV/d \ln r$ [$dV/d \ln r = 4/3\pi r^4 n(r)$] for $m_r = 1.30, 1.40, 1.50$. The small discrepancies exhibited by the size distribution retrieved by use of the true refractive index are due to method error. The size distributions inferred with other refractive indices depart from the exact distribution principally in the range of submicrometer particles. These adjustments of the number of small particles tend to compensate mainly for the variations of the scattering efficiency factor linked to the various guesses for m_r. For the large particles, the agreement is better because $n(r)$ is derived from forward directions where the scattered light corresponds principally to diffraction, which does not depend on the refractive index.

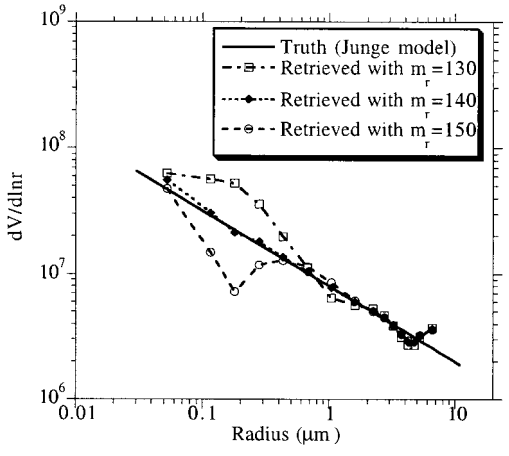

Fig. 10. Volume size distributions derived from the inversion of the retrieved phase function for various real refractive indices, including the true refractive index. The true size distribution (the Junge model) is also shown.

Table 1. rms Relative Deviation (×100) between Measured and Retrieved Phase Function σ_p, Spectral Optical Thickness σ_τ, and Polarized Phase Function σ_q as a Function of the Real Part of the Refractive Index Used in the Inversion of $n(r)$

	rms Relative Deviation (×100)				
m_r	1.30	1.35	1.40	1.45	1.50
σ_p, $\Theta < 20°$	0.015	0.015	0.021	0.019	0.026
σ_p, all Θ	0.033	0.011	0.005	0.009	0.033
σ_τ	6.80	4.35	0.30	5.65	12.00
σ_q	59.0	32.5	4.8	25.0	57.0

That this is so may be seen by the contribution of the size classes to the phase function in Fig. 9: Particles smaller than 0.1 μm (class 1) or with radii of 0.10–0.5 μm (classes 2–5) contribute the most to the phase function at large angles, whereas large particles, larger than 0.8 μm (above class 8), contribute exclusively to forward scattering.

To show how the retrieved size distribution fits the phase function, we show in Table 1 the rms residuals σ_p [Eq. (24)], between the true and the retrieved phase functions for the various choices for m_r. Two results are indicated: σ_p has been estimated only over scattering directions that correspond to the aureole range and then over all scattering directions, including large scattering angles. The results are similar and show that, whatever the choice for m_r, the retrieved size distribution fits the measurements quite perfectly. Alternatively, no information about the particle's refractive index can be obtained from simple radiance measurements at one wavelength, and the uncertainty in the size distribution in Fig. 10 cannot be reduced.

Multispectral radiance measurements can provide $p_A(\Theta)$ and ω_0 at several wavelengths, or, equivalently, $p_A(\Theta)$ and ω_0 at one wavelength complemented by the spectral dependence of the aerosol optical thickness, $\tau_A(\lambda)$. Then, besides the retrieval of the particle-size distribution, some indication of the particle's refractive index can be derived (see, e.g., Refs. 19–21). To illustrate this, we consider here that the previous measurements of the sky radiance at 870 nm are complemented by extinction measurements at N wavelengths ranging from 440 to 870 nm. The retrieval of the aerosol size distribution is performed as previously from $p_A(\Theta)$ for several values of m_r, but now the retrieved size distribution $n(r)$ allows us to calculate the expected optical thickness $\tau_A(\lambda)$ for comparison with the measurements. For the case of the Junge size distribution, the rms differences between the measured and the calculated optical thickness,

$$\sigma_\tau = \left\{ \frac{1}{N} \sum_{j=1}^{N} \left[\frac{\tau_A(\lambda_j) - \tau_A^{\text{cal}}(\lambda_j)}{\tau_A(\lambda_j)} \right]^2 \right\}^{1/2}, \qquad (25)$$

are listed in Table 1 as a function of the estimated refractive index. Note that m_r was considered spectrally flat (440–870 nm) in these calculations. The expected spectral variation of m_r for typical terrestrial aerosols within the visible range are probably small enough to be neglected,[36] but the spectral dependence of m_r is an issue raised by the method. In any case, the variation of σ_τ in Table 1 shows that retrieval of the aerosol's refractive index is possible from monospectral radiance measurements, provided that the $\tau_A(\lambda)$ measurements are accurate within a few percent.

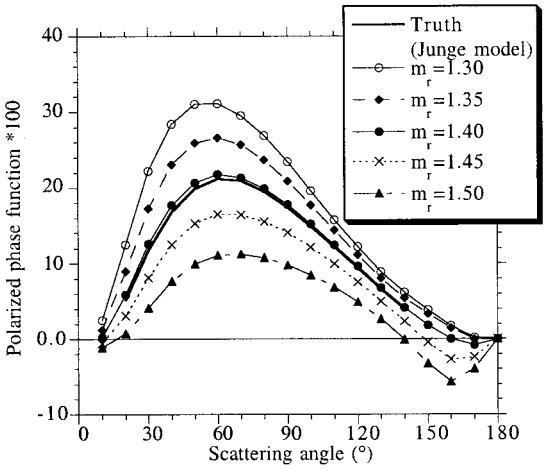

Fig. 11. True polarized phase function compared with calculations that correspond to various choices of m_r when the size distribution is inverted. The best fit between measurements and calculations yields the correct value of m_r.

2. *Retrieval from Combined Radiance and Polarized Radiance Measurements*

Finally, we consider detailed measurements that provide simultaneously the solar extinction, the sky radiance, and the polarized sky radiance values at one wavelength. We do not use the spectral dependence of $\tau_A(\lambda)$ in the inversion so that we may avoid any question of possible variation of the aerosol's refractive index.

Given m_r, let us first derive $n(r)$ from $p_A(\Theta)$, as was previously done. Then, from the retrieved size distribution and the corresponding refractive index, the aerosol polarized phase function $q_A(\Theta)$ is calculated and compared with the measurements. For the Junge-size distribution, Fig. 11 shows a comparison of the true polarized phase function and the calculations that correspond to the choices for m_r. The resultant rms values,

$$\sigma_q = \left\{ \frac{1}{N} \sum_{j=1}^{N} \left[\frac{q_A(\Theta_j) - q_A^{\text{cal}}(\Theta_j)}{q_A(\Theta_j)} \right]^2 \right\}^{1/2}, \qquad (26)$$

are listed in Table 1. The large variation of σ_q illustrates the sensitivity of polarization to the particle's refractive index. Table 1 shows that σ_q is ~10 times larger than σ_τ. Significant information about the particle's refractive index is embedded in the polarization measurements, and accordingly the best fit between measurements and calculations yields the correct value of m_r, here $m_r = 1.40$.

By applying the same analysis for the case of the

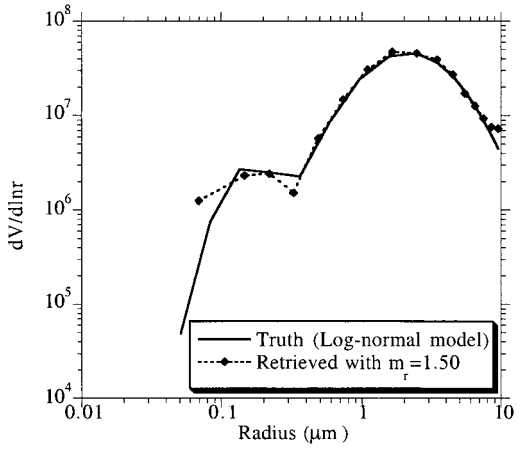

Fig. 12. Same as Fig. 10 but the true size distribution here corresponding to that of the bimodal log-normal model.

bimodal size distribution used in Subsection 2.C, we arrive at a retrieved refractive index of ~1.50, and the retrieved size distribution compares well with the exact one, as shown in Fig. 12.

The interest in polarization measurements for characterization of aerosols, especially of the aerosols' refractive indices, was documented long ago.[23,37] The sensitivity of polarization both to the particle's refractive index and its size distribution is elaborated below.

One could try to process the phase function only once by using some arbitrary refractive index (say, 1.50) to invert $n(r)$ and then performing Mie calculations of the polarized phase function with various m_r to search for a best fit. This method, however, generally has little chance of success. In the present case of the Junge distribution, inversion of $n(r)$ from

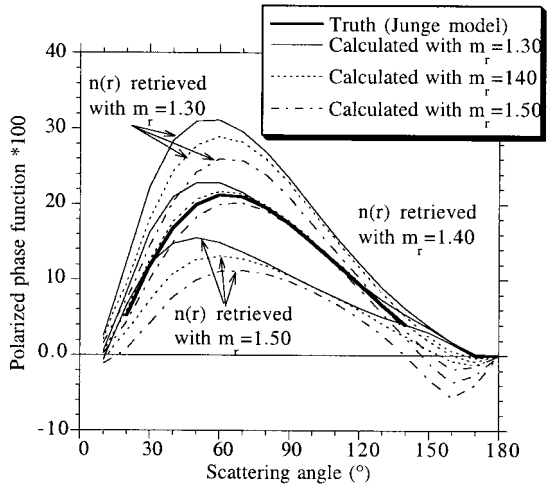

Fig. 13. $n(r)$ has been retrieved from $p_A(\Theta)$ with m_r = 1.30, 1.40, 1.50. In each case, given $n(r)$, we calculated the polarized phase functions for m_r = 1.30, 1.40, 1.50, as shown. The three lowest curves show polarized phase functions that correspond to Mie computations with three values of m_r with $n(r)$ obtained with m_r of 1.50. The three middle (upper) curves correspond to Mie computations with $n(r)$ obtained with m_r of 1.40 (1.30), and 3 values of m_r.

$p_A(\Theta)$ was performed successively with m_r = 1.30, 1.40, 1.50, and, in each case, given the retrieved $n(r)$, the polarized phase function was calculated for m_r = 1.30, 1.40, 1.50. The results are shown in Fig. 13. Figure 13 shows that, when a wrong guess is made for m_r (here m_r = 1.30 or m_r = 1.50) in the first inversion step, the systematic biases entailed in $n(r)$ make the further estimates of $q_A(\Theta)$ so inconsistent that comparison with the data gives no useful information on m_r. One must fit the whole data set by running the whole inversion of both the phase function and the polarized phase function with the correct refractive index of the particles.

A second point concerns the residual error in the retrieved polarized phase function (~5% in Table 1) in spite of the fact that the true value of the aerosol's refractive index was used (1.40). This discrepancy underscores again the sensitivity of polarized light to particle dimension, especially for very small particles. Because of the lesser sensitivity of $p_A(\Theta)$ to these small particles, the systematic errors in $n(r)$ (method errors) in this size range have a small but significant influence on the retrieval accuracy of $q_A(\Theta)$. To improve the results it is necessary to include polarization measurements in the $n(r)$ retrieval. A simple solution consists in complementing the K linear equations that correspond to the K values of $p_A(\Theta)$ in Eq. (19) by K' similar equations that correspond to K' measurements of $q_A(\Theta)$. Inversion of the $p_A(\Theta)$ and $q_A(\Theta)$ data set by this system of $[K + K']$ linear equations, when the true refractive index is used, allows one to retrieve quite exactly the true size distribution of the aerosols and thus to fit both $p_A(\Theta)$ and $q_A(\Theta)$. However, whereas the A_{ij} that correspond to the $p_A(\Theta)$ terms exhibit smooth behavior as a function of r and Θ, the behavior of the A_{ij} that correspond to $q_A(\Theta)$ is much more erratic, which can entail instabilities of the inversion. A procedure that avoids these instabilities consists of processing the inversion of $p_A(\Theta)$ as explained above, in a first step, with the system of $[K]$ equations, and to use the size distribution obtained in this way with the best choice of m_r to initialize $n(r)$ in Eq. (17) when one is processing the system of $[K + K']$ in a second step.

4. Conclusions

We have developed a method for retrieving the scattering and physical properties of aerosol particles. In addition to the commonly used spectral solar transmission and aureole measurements, the method exploits the advantage of intensity and polarization information by employing the sky radiance and the polarized sky radiance in the principal plane. The single-scattering albedo and the natural and polarized phase functions of the aerosols are retrieved from the solar extinction and from the total and polarized sky radiances after correction for multiple scattering, molecular scattering, and the influence of ground reflectance. The proposed scheme for retrieval of ω_0, $p_A(\Theta)$, and $q_A(\Theta)$ does not require any assumptions with respect to the aerosol properties.

The refractive index and the size distribution are then derived from the natural and polarized phase functions. It is shown that polarization is particularly useful for retrieving the real part of the refractive index. Comparison of retrievals conducted with and without polarization data shows that in some cases the inclusion of polarization in the size-distribution retrieval can improve information on the sizes of the smallest particles.

We have used simulated ground-based measurements under typical experimental conditions to test the performance of the method. A study of the sensitivity of the retrieved natural and polarized phase functions to the first-guess inputs of the scheme and to measurement errors was carried out. We found that an uncertainty of 10% in the measured total radiance does not significantly affect retrieval of the phase function (less than 2% error) and entails typically 2–10% errors in the polarized phase function for scattering angles below 120° and as many as 16% errors at 140°. Uncertainties in the aerosol optical thickness and surface reflectance have lesser effects on the retrieval.

The method has been applied with success to measurements at 870 nm.[33] Devaux *et al.*[18] used this method to characterize aerosol absorption. Examples of the aerosol polarized phase function retrieved from ground-based observations have been summarized by Herman *et al.*[5] We intend to detail these results in a future paper, in which we shall provide typical radiative and microphysical properties of different types of aerosol. Future studies should examine the extension of the method to shorter wavelengths, where the preponderance of the molecular contribution and the influence of the aerosol vertical mixing with molecules make solution of the problem of retrieving the properties of aerosols from ground-based measurements more difficult.

This research was supported by the Centre National d'Etudes Spatiales (France).

References

1. P. Y. Deschamps, F. M. Bréon, M. Leroy, A. Podaire, A. Bricaud, J. C. Buriez, and G. Sèze, "The POLDER mission: instrument characteristics and scientific objectives," IEEE Trans. Geosci. Remote Sens. **32,** 598–615 (1994).
2. Y. J. Kaufman, D. D. Herring, K. J. Ranson, and G. J. Collatz, "Earth observing system AM1 mission to Earth," IEEE Trans. Geosci. Remote Sens. **36,** 1045–1055 (1998).
3. D. Tanré, Y. J. Kaufman, M. Herman, and S. Mattoo, "Remote sensing of aerosol properties over oceans using the MODIS/EOS spectral radiances," J. Geophys. Res. **102,** 16971–16988 (1997).
4. J. V. Martonchik, D. J. Diner, R. A. Kahn, T. P. Ackerman, M. E. Verstraete, B. Pinty, and H. R. Gordon, "Techniques for the retrieval of aerosol properties over land and ocean using multiangle imaging," IEEE Trans. Geosci. Remote Sens. **36,** 1212–1227 (1998).
5. M. Herman, J. L. Deuzé, C. Devaux, P. Goloub, F. M. Bréon, and D. Tanré, "Remote sensing of aerosols over land surfaces including polarization measurements and application to POLDER measurements," J. Geophys. Res. **102,** 17039–17049 (1997).
6. Y. J. Kaufman, D. Tanré, H. R. Gordon, T. Nakajima, J. Lenoble, R. Frouin, H. Grassl, B. M. Herman, M. D. King, and P. M. Teillet, "Passive remote sensing of tropospheric aerosol and atmospheric correction for the aerosol effect," J. Geophys. Res. **102,** 16815–16830 (1997).
7. E. F. Vermote, N. Z. El Saleous, C. O. Justice, Y. J. Kaufman, L. Remer, J. C. Roger, and D. Tanré, "Atmospheric correction of visible to middle infrared EOS-MODIS data over land surface, background, operational algorithm and validation," J. Geophys. Res. **102,** 17131–17141 (1997).
8. B. N. Holben, T. F. Eck, I. Slutsker, D. Tanré, J. P. Buis, A. Setzer, E. Vermote, J. A. Reagan, Y. J. Kaufman, T. Nakajima, F. Lavenu, I. Jankowiak, and A. Smirnov, "AERONET—a federated instrument network and data archive for aerosol characterization," Remote Sens. Environ. **66,** 1–16 (1998).
9. M. D. King, D. M. Byrne, B. M. Herman, and J. A. Reagan, "Aerosol size distributions obtained by inversion of spectral optical depth measurements," J. Atmos. Sci. **35,** 2153–2167 (1978).
10. G. E. Shaw, "Inversion of optical scattering and spectral extinction measurements to recover aerosol size spectra," Appl. Opt. **18,** 988–993 (1979).
11. M. A. Box and A. Deepak, "Retrieval of aerosol size distribution by inversion of solar aureole data in the presence of multiple scattering," Appl. Opt. **18,** 1376–1382 (1979).
12. J. T. Twitty, "The inversion of aureole measurements to derive aerosol size distribution," J. Atmos. Sci. **32,** 584–591 (1975).
13. N. T. O'Neill and J. R. Miller, "Combined solar aureole and solar beam extinction measurements. 2. Studies of the inferred aerosol size distribution," Appl. Opt. **23,** 3697–3704 (1984).
14. D. Tanré, C. Devaux, M. Herman, R. Santer, and J. Y. Gac, "Radiative properties of desert aerosols by optical ground-based measurements at solar wavelengths," J. Geophys. Res. **93,** 14223–14231 (1988).
15. Y. J. Kaufman, A. Gitelson, A. Karnieli, E. Ganor, R. S. Fraser, T. Nakajima, S. Mattoo, and B. N. Holben, "Size distribution and scattering phase function of aerosol particles retrieved from sky brightness measurements," J. Geophys. Res. **99,** 10341–10356 (1994).
16. T. Nakajima, M. Tanaka, and T. Yamauchi, "Retrieval of the optical properties of aerosols from aureole and extinction data," Appl. Opt. **22,** 2951–2959 (1983).
17. M. Wang and H. R. Gordon, "Retrieval of the columnar aerosol phase function and single scattering albedo from sky radiance over the ocean: simulations," Appl. Opt. **32,** 4598–4609, (1993).
18. C. Devaux, A. Vermeulen, J. L. Deuzé, P. Dubuisson, M. Herman, R. Santer, and M. Verbrugghe, "Retrieval of aerosol single-scattering albedo from ground-based measurements: application to observational data," J. Geophys. Res. **103,** pp. 8753–8761 (1998).
19. T. Nakajima, G. Tonna, R. Rao, P. Boi, Y. Kaufman, and B. Holben, "Use of sky brightness measurements from ground for remote sensing of particulate dispersion," Appl. Opt. **35,** 2672–2686 (1996).
20. M. Wendisch, and W. von Hoyningen-Huene, "Possibility of refractive index determination of atmospheric aerosol particles by ground-based solar extinction and scattering measurements," Atmos. Environ. **28,** 785–792 (1994).
21. P. Romanov, N. T. O'Neill, A. Royer, and B. McArthur, "Simultaneous retrieval of aerosol refractive index and particule size distribution from ground based measurements of direct and scattered radiation," Appl. Opt. **38,** 7305–7320 1999.
22. J. E. Hansen and L. D. Travis, "Light scattering in planetary atmospheres," Space Sci. Rev. **16,** 527–610 (1974).
23. Z. Sekera, "Light scattering in the atmosphere and the polarization of sky light," J. Opt. Soc. Am. **47,** 484–490 (1957).

24. R. Eiden, "Determination of the complex index of refraction of spherical aerosol particles," Appl. Opt. **10,** 749–754 (1971).
25. M. I. Mishchenko and L. D. Travis, "Satellite retrieval of aerosol properties over the ocean using polarization as well as intensity of reflected sunlight," J. Geophys. Res. **102,** 16989–17013 (1997).
26. B. M. Herman, S. R. Browning, and R. J. Curran, "The effect of atmospheric aerosols on scattered sunlight," J. Atmos. Sci. **28,** 419–428 (1971).
27. J. L. Deuzé, C. Devaux, M. Herman, R. Santer, and D. Tanré, "Saharan aerosols over the south of France: characterization derived from satellite data and ground based measurements," J. Appl. Meteorol. **27,** 680–686 (1988).
28. J. L. Deuzé, C. Devaux, M. Herman, R. Santer, J. Y. Balois, L. Gonzalez, P. Lecomte, and C. Verwaerde, "Photopolarimetric observations of aerosols and cloud from balloon," Remote Sens. Environ. **29,** 93–110 (1989).
29. B. Cairns, B. E. Carlson, A. A. Lacis, and E. E. Russell, "An analysis of ground-based polarimetric sky radiance measurements," in *Polarization: Measurement, Analysis, and Remote Sensing*, R. A. Chipman and D. H. Goldstein, eds., Proc. SPIE **3121,** 383–393 (1997).
30. S. Chandrasekhar, *Radiative Transfer* (Oxford U. Press, Oxford, 1950) [Dover, New York, (1960)].
31. J. E. Hansen, "Multiple scattering of polarized light in planetary atmospheres. II. Sunlight reflected by terrestrial water clouds," J. Atmos. Sci. **28,** 1400–1426 (1971).
32. J. L. Deuzé, M. Herman, and R. Santer, "Fourier series expansion of the transfer equation in the atmosphere–ocean system," J. Quant. Spectros. Rad. Transfer **41,** 483–494 (1989).
33. A. Vermeulen, "Caractérisation des aérosols à partir de mesures optiques passives au sol: apport des luminances totale et polarisée dans le plan principal," Ph.D. dissertation (Université des Sciences et Technologies de Lille, Lille, France 1996).
34. F. M. Bréon, D. Tanré, P. Lecomte, and M. Herman, "Polarized reflectance of bare soils and vegetation: measurements and models," IEEE Trans. Geosci. Remote Sens. **33,** 487–499 (1995).
35. B. Lafrance, "Modélisation simplifiée de la lumière polarisée émergeant de l'atmosphère. Correction de l'impact des aérosols stratosphériques sur les mesures de POLDER, "Thèse (Université des Sciences et Technologies de Lille, Lille, France, 1997).
36. G. A. D'Almeida, P. Koepke, and E. P. Shettle, *Atmospheric Aerosols, Global Climatology and Radiative Characteristics* (Deepak, Hampton, Va., 1991).
37. J. E. Hansen and J. M. Hovenier, "Interpretation of the polarization of Venus," J. Atmos. Sci. **31,** 1137–1160 (1974).
38. R. Santer and M. Herman, "Particle size distribution from forward scattered light using the Chahine inversion scheme," Appl. Opt. **22,** 2294–2302 (1983).